Int. J. Fuzzy Syst. (2019) 21(8):2542–2555
https://doi.org/10.1007/s40815-019-00739-2

Cooperative Localization Using Fuzzy DDEIF and Broad Learning System for Uncertain Heterogeneous Omnidirectional Multi-robots

Ching-Chih Tsai[1] · Ching-Fu Hsu[1] · Chung-Wei Wu[1] · Feng-Chun Tai[1]

Received: 8 March 2019 / Revised: 9 June 2019 / Accepted: 3 September 2019 / Published online: 1 October 2019

Abstract This paper presents a novel fuzzy distributed and decentralized extended information filtering (FDDEIF) method using broad learning system (BLS), called BLS-FDDEIF, for indoor cooperative localization of a group of heterogeneous omnidirectional mobile robots (HOMRs) incorporated with their dynamic effects. A new pose initialization algorithm is proposed to estimate the robots' initial poses. Once all the initial poses of the HOMRs have been roughly determined, a novel BLS-FDDEIF method is presented to fuse multisensory measurements for estimating more accurate poses of all the HOMRs. Comparative simulations and experimental results are conducted to show the effectiveness and superiority of the proposed method in finding accurate pose estimation of three cooperative HOMRs with unknown initial poses.

Keywords Broad learning system (BLS) · Cooperative localization · Fuzzy distributed and decentralized extended information filtering (FDDEIF) · Multi-robots · Heterogeneous omnidirectional mobile robot (HOMR)

1 Introduction

Multi-robot systems have received much attention in intelligent control and smart automation communities or professional societies due to their many successful applications, such as industrial manufacturing, human servicing, smart agriculture, cooperative material handling via multi-robots, and so on. Such systems or robots have been mainly employed to reduce human interventions in doing numerous dangerous, repeated, boring, and difficult tasks. In general, interactions among multi-robots can be classified into five technical categories: collective, cooperative, collaborative, coordinative, and adversary [1]. Worthy of mention is that, in the cooperative interaction, mobile robots help each other and cooperate with each other to achieve their common or shared goal. This cooperative control method has been widely used in many applications, such as Intel's 500 Drones, artificial satellites, and service robot in a team. Cooperative multi-robot systems have been shown to perform tasks, which cannot be done by a single mobile robot, or such task can be completed or accomplished more efficiently by exchanging information among robots.

Recently, cooperative localization of a group of mobile multi-robots has also attracted considerable attention in control and robotics communities. This technology is concerned with two technical issues: one is group pose initialization which means to find initial poses of all multi-robots in a team, and the other is group pose tracking which is related to keep track of moving poses of all multi-robots. The authors in [2] proposed a FDDEIF method with a modified graph theory for cooperative localization of a class of mobile wheeled multi-robots by addressing both issues of group pose initialization and group pose tracking. Furthermore, Tan [3] proposed a two cooperative global localization methods using fuzzy decentralized extended information filtering (FDEIF) and fuzzy decentralized extended Kalman filtering (FDEKF) for global cooperative positioning of a multi-ballbot system in the case of known maps. Yang [4] addressed the group pose initialization and tracking problems using fuzzy distributed and decentralized extended information filtering (FDDEIF) for a team of

✉ Ching-Chih Tsai
cctsai@nchu.edu.tw

[1] Department of Electrical Engineering, National Chung Hsing University, Taichung, Taiwan, ROC

omnidirectional mobile robots. Wang and de Silva [5] presented decentralized Kalman filters to achieve cooperative transportation of multiple robots for group pose tracking. However, those methods in [1–5] for cooperative localization of a class of mobile multi-robots has not considered the dynamic effect of each mobile robot yet.

Neural networks have been widely used for nonlinear system identification and control; for example, recurrent fuzzy wavelet neural networks were exploited to achieve trajectory tracking of a tilting quadrotor [6]. Recently, broad learning system (BLS) has been proposed as an original flat structure established based on the random vector functional-link neural network (RVFLNN), which inherits its major features [7]; this type of system can be expanded in a wide sense [7]. Chen et al. [8] further discussed the general approximation capability and nonlinear system of BLS and some variants with their mathematical models. BLS is indeed different from some popular deep neural networks, which have high computing cost and suffer from a time consuming learning for excessive parameters, thereby providing a much faster method with high accuracy. In applying BLS, Feng and Chen [9] applied BLS with an iterative gradient decent algorithm to propose a BLS control method for a class of nonlinear dynamic system, and Tsai et al. [10] combined BLS and fractional-order nonsingular terminal siding-mode control to accomplish a nonlinear consensus formation control for a kind of heterogeneous omnidirectional robots. Motivated by [8–10], the BLS would be helpful in learning unknown dynamic uncertainties in real time.

Omnidirectional mobile robots (OMRs) have been widely used for our living life and industrial applications. There are two kinds of Swedish or Mecanum wheels, which are, respectively, 45° and 90° [11, 12]. Unlike conventional differential driving, OMRs have the superior flexibility to move towards any position and orientation. Owing to both wheel structures, OMRs can be made using different wheel configurations including three wheels, four wheels, car-like four wheels, etc. In [13], the authors proposed a consensus-based formation control method for heterogeneous OMRs (HOMRs) which are OMRs with different wheel configurations and distinct dynamics by finding their unified dynamic models. Inspired by [4, 8–10, 13], it would be theoretically and practically interesting to combine FDDEIF and BLS to address the group pose initialization, pose, and pose rate estimation problems for a team of HOMRs incorporated with uncertain dynamic effects.

Hence, the objective of this paper is to combine the graph-based FDDEIF method and BLS for developing a new BLS-FDDEIF method to address both group global pose initialization and moving pose estimation problems for a dynamic multi-HOMR system whose communication network is not fully connected. By comparing to existing methods, the presented contents are delineated in two technical contributions. One is a novel BLS-FDDEIF proposed for cooperative pose initialization and dynamic pose tracking of a group of HOMRs, where the iterative learning algorithms for each BLS have been proposed to online learn an uncertain term in the dynamic model of each HOMR incorporated with dynamic effects and uncertainties. The other is numerical and experimental verification of the proposed BLS-FDDEIF approach via computer simulations and experimental results of a physical multi-HOMR system.

The rest of the paper is outlined as follows. Section 2 briefly recalls the measurement models of HOMRs. Section 3 proposes the BLS identifier to learn the uncertain dynamic part of each HOMR with dynamic effects and uncertainties. Section 4 introduces the DDEIF method for mobile multi-robot systems, and then describes the FDDEIF algorithm with the fuzzy tuner. Section 5 proposes the cooperative pose initialization algorithm to corporately initialize the poses of all the HOMRS. Section 6 presents the proposed BLS-FDDEIF algorithm for dynamic localization of the multi-HOMR system. Computer simulations are performed in Section 7 to show the effectiveness and superiority of the proposed BLS-FDDEIF algorithm. Section 8 shows and discusses two experiment results. Finally, Section 9 concludes this paper.

2 Measurement Models of HOMRs

This section is to recall the models of the RGB-D sensor and laser scanner mounted on the three kinds of HOMRs, which are, respectively, four-wheeled OMR (FOMR), car-like OMR (COMR), and three-wheeled OMR (TOMR), as shown in Fig. 1a–c, since each HOMR is equipped with one RGB-D sensor, one laser scanner, and appropriate numbers of encoders on its driving wheels. The basic dead-reckoning or odometry of each HOMR, based on the corresponding encoders' outputs and kinematic models, is described in [13] and not mentioned here.

2.1 RGB-D Sensor Model

RGB-D sensor is equipped with one RGB camera and a pair of depth sensors. The RGB-D sensor is mounted on each HOMR at its designed height, where Fig. 1a–c show the used Realsense D415 RGB-D sensor. In the measurement update step, each HOMR detects landmarks around it in order to estimate its pose. Via the RGB-D measurements and the used landmark detection procedure in [2, 4], it is easy to calculate the azimuth angle α_{ij} with respect to the heading direction of the ith HOMR and the distance λ_{ij} to

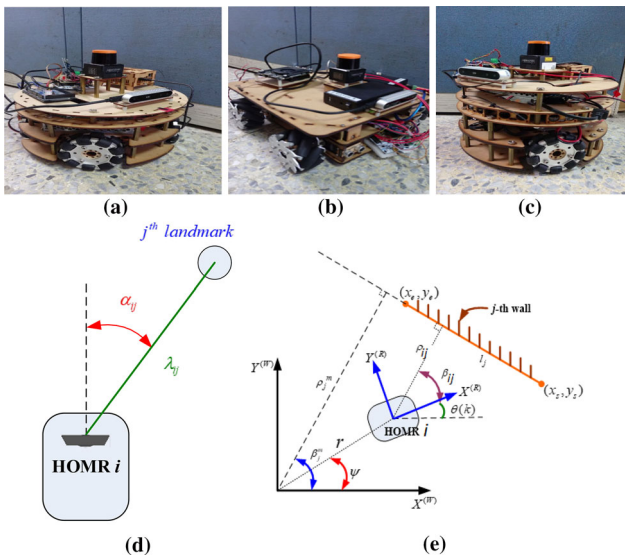

Fig. 1 Three HOMRs and sensor models. **a** Four-wheeled OMR (FOMR). **b** Car-like OMR (COMR). **c** Three-wheeled OMR (TOMR). **d** Parameters defining the *j*th landmark. **e** Parameters defining the *j*th wall

the *j*th landmark $L_j(x_L, y_L, z_L)$ as shown in Fig. 1d at time instant k. The value of the measurement function for the *j*th landmark from HOMR i is expressed by

$$z_{\mathrm{RGBD_{ij}}}(k) = h_{\mathrm{RGBD_{ij}}}(X(k), L_i) = \begin{bmatrix} \alpha_{ij} \\ \lambda_{ij} \end{bmatrix} = \begin{bmatrix} \tan^{-1}\dfrac{y_{L_j} - y_i(k)}{x_{L_j} - x_i(k)} - \theta_i(k) \\ \sqrt{\left(x_{L_j} - x_i(k)\right)^2 + \left(y_{L_j} - y_i(k)\right)^2 + \left(z_{L_j} - z_i(k)\right)^2} \end{bmatrix} + V_{\mathrm{RGBD_{ij}}}(k) \tag{1}$$

where $x_i(k)$, $y_i(k)$, $z_i(k)$, $\theta_i(k)$ represents the pose coordinates of the *i*th HOMR in the world frame; note that $V_{\mathrm{RGBD}_{ij}}(k)$ is the zero-mean measurement noise vector with zero mean and diagonal covariance matrix $R_{\mathrm{RGBD}_{ij}}(k)$. Note that the azimuth angle α_{ij} is negative in the clockwise direction.

2.2 Laser Scanner

In order to localize each HOMR by the laser scanner, UST-10LX, from Hokuyo, we here adopt the well-known minimalistic environment model, which is composed of a set of walls, m_j i.e., $\mathbf{M} = \{m_j, j = 1, \ldots, \overline{M}\}$. Figure 1e illustrates the parameters which define the *j*th wall, where (x_e, y_e) and (x_s, y_s) are the ending and starting points of the *j*th wall, l_j is the length of the *j*th wall, ρ_j^m is the perpendicular distance from the origin in the world frame to the *j*th wall, and β_j^m stands for the orientation of the *j*th wall. Distance measurements can be obtained from the laser ranging data in one whole scanning cycle. Therefore, the measurement model of the laser scanner for HOMR i is expressed by [2, 4]

$$z_{\mathrm{laser}i}(k) = \bar{h}_{\mathrm{laser}i}(X_i(k), \mathbf{M}) + V_{li}(k) \tag{2}$$

where $\bar{h}_{\mathrm{laser}}(X_i, \mathbf{M}) = \left[\bar{h}_{\mathrm{laser}_{i1}}(X_i, m_1) \ldots \bar{h}_{\mathrm{laser}_{i\overline{M}}}(X_i, m_{\overline{M}})\right]^{\mathrm{T}}$, $X_i(k) = [x_i\, y_i(k)\, \theta_i(k)]^{\mathrm{T}}$, $V(k) = \left[v_1(k) \quad v_2(k) \quad \ldots \quad v_{\overline{M}}(k)\right]^T$, and $\overline{M}$ denotes the number of the total walls. Note that $V_{1i}(k)$ denote is the measurement noise vector with zero mean and covariance matrix $R_{li}(k) = \mathrm{diag}\{\delta_1^2, \delta_2^2, \ldots, \delta_{\overline{M}}^2\}$. Moreover, the measurement function $\bar{h}_{\mathrm{laser}_i}(X_i, m_j)$ is described by

$$\bar{h}_{\mathrm{laser_{ij}}}(X_i, m_j) = \begin{bmatrix} \rho_{ij} \\ \beta_{ij} \end{bmatrix} \tag{3}$$

where

$$\rho_{ij} = \rho_j^m - \sqrt{x_i^2 + y_i^2}\cos\left(\alpha_j^m - \psi\right) = \rho_j^m - \left(x_i \cos\alpha_j^m + y_i \sin\alpha_j^m\right)$$
$$\beta_{ij} = \beta_j^m - \theta_i,\ j = 1, 2, 3, \ldots, \overline{M}.$$

3 BLS Identifier for Dynamic Model of Each HOMR with Dynamic Effect and Uncertainties

This section will introduce the nonlinear discrete-time stochastic system model of the multi-HOMR system with one set of measurement models, and construct a BLS identifier to online learn the dynamic term of each HOMR with dynamic effects and uncertainties. The unified dynamic model of HOMR proposed in [13] will be used. In particular, the iterative learning algorithm of a BLS identifier will be derived based on the well-known gradient descent method.

3.1 Modeling of Multi-HOMRs with Dynamic Effects

Since the multi-HOMR system is composed of N HOMRs, the dynamic behavior model of the *i*th HOMR with one RGB-D sensor and one laser scanner is modeled by a nonlinear discrete-time stochastic system model with one measurement model expressed by [13]

$$\begin{bmatrix} x_i(k+1) \\ v_i(k+1) \end{bmatrix} = \begin{bmatrix} x_i(k) + Tv_i(k) \\ T \cdot (-g_i(k) + \xi_i(k)) + Tu_i(k) \end{bmatrix} \tag{4}$$

or in a vector–matrix form

$$X_i(k+1) = f_i(X_i(k), u(k)) + \begin{bmatrix} 0 \\ T\xi_i(k) \end{bmatrix} \tag{5}$$

$$Z_i(k) = h_i(X_i(k), \mathbf{L}, \mathbf{M}, k) + V_i(k) \tag{6}$$

where $\mathbf{L}$ denotes the set of all landmarks; $x_i(k) \in R^3$, $v_i(k) \in R^3$; $X_i(k+1) = [x_i(k+1)\ \ v_i(k+1)]^{\mathrm{T}} \in R^6$; $h_i(\cdot) \in R^P$

are nonlinear, twice differentiable functions of the system state; $u_i(k) \in R^3$ means the input of the ith HOMR. The stochastic process vectors, $\xi_i(k) \sim N(0, Q_i(k))$ and $V_i(k) \sim N(0, R_i(k))$ are the process noise and the measurement noise, respectively. Note that $h_i(X_i(k), \mathbf{L}, \mathbf{M}, k)$ is the combination of the measurement models of the RGB-D camera and laser scanner. Since the nonlinear term, $g_i(k)$, is unknown, the BLS will be used to online learn the nonlinear term, $g_i(k)$, based on the gradient descent method in the coming subsection.

3.2 BLS Approximation

This subsection will propose iterative learning algorithms for BLS to learn online and approximate the nonlinear term, $g_i(k)$, in (4). The proposed iterative learning algorithms are based on the gradient descent method; the algorithms first find the gradients of all the updating parameters in the used BLS as shown in Fig. 2, and then use the deepest descent approach to obtaining the iterative parameter learning rules or algorithms. In doing so, suppose that there are n mapping groups with K_i feature nodes in the ith group, and there are one group of m enhancement nodes, the input vector is denoted $\mathbf{X}_l$, $l = 1, \ldots, M$, and the BLS output vector is denoted as $\hat{y}$.

$$\hat{y} = \sum_{i=1}^{n}\sum_{k=1}^{K_i} w_k^i F_k^i + \sum_{j=1}^{m} w_j \xi_j \left(\sum_{i=1}^{n}\sum_{k=1}^{K_i} w_{jk}^i F_k^i + b_j \right) \tag{7}$$

where $F_k^i = \phi_k^i\left(\sum_{l=1}^{M}\left(w_{f_{kl}}^i \mathbf{X}_l + b_{f_k}^i\right)\right)$ denotes the output of the kth feature node in the ith mapping group, $\phi_k^i(\bullet)$ and $\xi_j(\bullet)$ is the activation function. We denote $W_{fi} = [w_{fkl}^i]_{M\times K_i}$, $\beta_{fi} = [b_{fk}^i]_{1\times K_i}$, $W_e = [w_{jk}^i]_{(K_1+K_2+\cdots+K_n)\times m}$, $\beta_e = [b_j]_{1\times m}$, where $w_{f_{kl}}^i$ is the weight connecting the lth input x_l to the kth feature node in the ith mapping group, $b_{f_k}^i$ is the bias term associated to the kth feature node in the ith mapping group, w_{jk}^i is the weight connecting the kth feature node of the ith mapping group to the jth enhancement node, and b_j is the bias term associated to the jth enhancement node. We define the weight matrix connecting the outputs of feature nodes and enhancement nodes to the output neuron as $W = \left[w_1^1, \ldots w_{K_1}^1, \ldots, w_n^n, \ldots w_{K_n}^n, w_1, \ldots, w_m\right]^{\mathrm{T}}$ where w_k^i is the weight connecting the kth feature node in the ith mapping group to the output neuron, and w_j is the weight connecting the jth enhancement node to the output neuron.

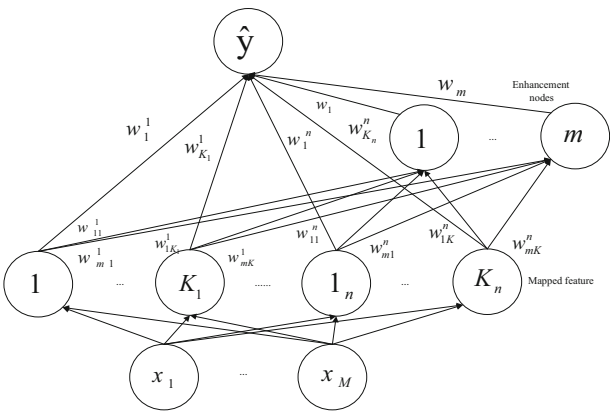

Fig. 2 Structure of the BLS

Next, derive the learning laws for the six types of parameters, $w_{f_{kl}}^i$, $b_{f_k}^i$, w_{jk}^i, b_j, w_k^i, w_j, according to the gradient descent method in the following six steps. First, the learning law for $w_{f_{kl}}^i$ is

$$\begin{aligned} w_{fkl}^i(k+1) &= w_{fkl}^i(k) - \eta \frac{\partial E(k)}{\partial w_{fkl}^i} \\ &= w_{fkl}^i(k) + \eta(y(k) - \hat{y}(k)) \frac{\partial \hat{y}(k)}{\partial w_{fkl}^i} \end{aligned} \tag{8}$$

where $E(k) = (y(k) - \hat{y}(k))^2/2$,

$$\hat{y} = \sum_{i=1}^{n}\sum_{k=1}^{K_i} w_k^i F_k^i + \sum_{j=1}^{m} w_j \xi_j \left(\sum_{i=1}^{n}\sum_{k=1}^{K_i} w_{jk}^i F_k^i + b_j \right),$$

and

$$\begin{aligned} \frac{\partial \hat{y}(k)}{\partial w_{fkl}^i} &= \frac{\partial \sum_{i=1}^{n}\sum_{k=1}^{K_i} w_k^i F_k^i}{\partial F_k^i(k)} \frac{\partial F_k^i(k)}{\partial\left(\sum_{l=1}^{K_i} w_{fkl}^i x_l + b_{fk}^i\right)} \\ &\quad \frac{\partial\left(\sum_{l=1}^{K_i} w_{fkl}^i x_l + b_{fk}^i\right)}{\partial w_{fkl}^i} \\ &\quad + \sum_{j=1}^{m} w_j \frac{\partial \xi_j(k)}{\partial\left(\sum_{i=1}^{n}\sum_{k=1}^{K_i} w_{jk}^i F_k^i + b_j\right)} \\ &\quad \frac{\partial\left(\sum_{i=1}^{n}\sum_{k=1}^{K_i} w_{jk}^i F_k^i + b_j\right)}{\partial F_k^i(k)} \frac{\partial F_k^i(k)}{\partial\left(\sum_{l=1}^{K_i} w_{fkl}^i x_l + b_{fk}^i\right)} \\ \frac{\partial\left(\sum_{l=1}^{K_i} w_{fkl}^i x_l + b_{fk}^i\right)}{\partial w_{fkl}^i} &= w_k^i \dot{\phi}_k^i x_l + \sum_{j=1}^{m} w_j \dot{\xi}_j w_{jk}^i \dot{\phi}_k^i x_l \\ &= \left(w_k^i + \sum_{j=1}^{m} w_j \dot{\xi}_j w_{jk}^i\right) \dot{\phi}_k^i x_l \end{aligned}$$

Second, the learning law for $b_{f_k}^i$ is

$$\begin{aligned} b_{fk}^i(k+1) &= b_{fk}^i(k) - \eta \frac{\partial E(k)}{\partial b_{fk}^i} \\ &= w_k^i(k) + \eta(y(k) - \hat{y}(k)) \frac{\partial \hat{y}(k)}{\partial b_{fk}^i} \end{aligned} \tag{9}$$

where

$$\frac{\partial \hat{y}(k)}{\partial b_{fk}^i} = \frac{\partial \sum_{i=1}^{n}\sum_{k=1}^{K_i} w_k^i F_k^i}{\partial F_k^i(k)} \frac{\partial F_k^i(k)}{\partial\left(\sum_{l=1}^{K_i} w_{fkl}^i x_l + b_{fk}^i\right)} \frac{\partial\left(\sum_{l=1}^{K_i} w_{fkl}^i x_l + b_{fk}^i\right)}{\partial b_{fk}^i} + \sum_{j=1}^{m} w_j \frac{\partial \xi_j(k)}{\partial\left(\sum_{i=1}^{n}\sum_{k=1}^{K_i} w_{jk}^i F_k^i + b_j\right)} \frac{\partial\left(\sum_{i=1}^{n}\sum_{k=1}^{K_i} w_{jk}^i F_k^i + b_j\right)}{\partial F_k^i(k)} \frac{\partial F_k^i(k)}{\partial\left(\sum_{l=1}^{K_i} w_{fkl}^i x_l + b_{fk}^i\right)}$$

$$\frac{\partial\left(\sum_{l=1}^{K_i} w_{fkl}^i x_l + b_{fk}^i\right)}{\partial b_{fk}^i} = w_k^i \dot{\phi}_k^i + \sum_{j=1}^{m} w_j \dot{\xi}_j w_{jk}^i \dot{\phi}_k^i = \left(w_k^i + \sum_{j=1}^{m} w_j \dot{\xi}_j w_{jk}^i\right)\dot{\phi}_k^i$$

Third, the learning law for w_{jk}^i is

$$w_{jk}^i(k+1) = w_{jk}^i(k) - \eta \frac{\partial E(k)}{\partial w_{jk}^i} = w_{jk}^i(k) + \eta(y(k) - \hat{y}(k)) \frac{\partial \hat{y}(k)}{\partial w_{jk}^i} \tag{10}$$

where

$$\frac{\partial \hat{y}(k)}{\partial w_{jk}^i} = \frac{\partial \hat{y}}{\partial \xi_j} \cdot \frac{\partial \xi_j}{\partial w_{jk}^i} = w_j \dot{\xi}_j \left(\sum_{i=1}^{n}\sum_{k=1}^{K_i} w_{jk}^i F_k^i + b_j\right) F_k^i$$

Fourth, the learning law for b_j is

$$w_k^i(k+1) = w_k^i(k) - \eta \frac{\partial E(k)}{\partial w_k^i} = w_k^i(k) + \eta(y(k) - \hat{y}(k)) \frac{\partial \hat{y}(k)}{\partial w_k^i} \tag{11}$$

where

$$\frac{\partial \hat{y}(k)}{\partial w_k^i} = F_k^i \text{ and } \frac{\partial E(k)}{\partial w_k^i} = \frac{\partial E}{\partial \hat{y}} \cdot \frac{\partial \hat{y}}{\partial w_k^i} = (\hat{y} - y) F_k^i$$

Finally, the learning law for w_j is

$$w_j(k+1) = w_j(k) - \eta \frac{\partial E(k)}{\partial w_j} = w_j(k) + \eta(y(k) - \hat{y}(k)) \frac{\partial \hat{y}(k)}{\partial w_j} \tag{12}$$

where

$$\frac{\partial \hat{y}(k)}{\partial w_j} = \xi_j \left(\sum_{i=1}^{n}\sum_{k=1}^{K_i} w_{jk}^i F_k^i + b_j\right).$$

Remark 1 Let $\xi_j(x) = \tan h\,(x) = \frac{e^x - e^{-x}}{e^x + e^{-x}}$, which gives $\dot{\xi}_j(x) = 1 - \xi_j^2(x)$.

Remark 2 Let $\phi_k^i(x) = x$, which obtains $\dot{\phi}_k^i(x) = 1$.

In what follows, the Lyapunov function is proposed to investigate the convergent condition of the BLS identifier. Let $\eta(k)$ be the learning rate at discrete time k for the BLS parameters. The BLS identifier is asymptotically convergent provided that η satisfies the following condition:

$$0 < \eta < \frac{2}{\max_k \left\| \left(\frac{\partial \hat{y}(k)}{\partial P(k)}\right) \right\|_2^2} \tag{13}$$

where $P(k) = \left[w_{fkl}^i \quad b_{fk}^i \quad w_k^i \quad w_j \quad w_{jk}^i \quad b_j \right]^{\mathrm{T}}$, and $\left\| \left(\frac{\partial \hat{y}(k)}{\partial P(k)}\right) \right\|_2^2$ is given as below.

$$\left\| \left(\frac{\partial \hat{y}(k)}{\partial P(k)}\right) \right\|_2^2 = \sum_{i=1}^{n}\sum_{k=1}^{K_i} \left(\left(\frac{\partial \hat{y}(k)}{\partial w_{fkl}^i}\right)^2 + \left(\frac{\partial \hat{y}(k)}{\partial b_{fk}^i}\right)^2 \right) + \sum_{j=1}^{m} \left(\left(\frac{\partial \hat{y}(k)}{\partial b_j}\right)^2 + \left(\frac{\partial \hat{y}(k)}{\partial w_j}\right)^2 \right) + \sum_{i=1}^{n}\sum_{k=1}^{K_i} \left(\left(\frac{\partial \hat{y}(k)}{\partial w_k^i}\right)^2 + \left(\frac{\partial \hat{y}(k)}{\partial w_{jk}^i}\right)^2 \right) \tag{14}$$

Using the previous BLS learning algorithms, one obtains

$$\begin{aligned} \Delta P(k) &= P(k+1) - P(k) \\ &= \eta(y(k) - \hat{y}(k)) \left[\frac{\partial \hat{y}(k)}{\partial w_{fkl}^i(k)} \quad \frac{\partial \hat{y}(k)}{\partial b_{fk}^i(k)} \quad \frac{\partial \hat{y}(k)}{\partial w_k^i(k)} \quad \frac{\partial \hat{y}(k)}{\partial w_j(k)} \quad \frac{\partial \hat{y}(k)}{\partial w_{jk}^i(k)} \quad \frac{\partial \hat{y}(k)}{\partial b_j(k)} \right]^{\mathrm{T}} \cdot \\ &= \eta e(k) \frac{\partial \hat{y}(k)}{\partial P(k)} \end{aligned} \tag{15}$$

Proof To prove the asymptotical convergence of the proposed BLS identifier, we choose the following Lyapunov function.

$$L(k) = (y(k) - \hat{y}(k))^2 = e^2(k) \tag{16}$$

Then the time difference of the Lyapunov function is given by

$$\Delta L_M(k) = L_M(k+1) - L_M(k) = \Delta e(k) \cdot [2e(k) + \Delta e(k)] \tag{17}$$

where

$$\begin{aligned}\Delta e(k) &= \left(\frac{\partial e(k)}{\partial P(k)}\right)^{\mathrm{T}} \Delta P(k) = \eta\left(\frac{\partial(y(k)-\hat{y}(k))}{\partial P(k)}\right)^{\mathrm{T}} \\ &\quad (y(k)-\hat{y}(k))\frac{\partial \hat{y}(k)}{\partial P(k)} \\ &= -\eta\frac{\partial \hat{y}(k)}{\partial P(k)}^{\mathrm{T}} e(k)\frac{\partial \hat{y}(k)}{\partial P(k)} = -\eta e(k)\frac{\partial \hat{y}(k)}{\partial P(k)}^{\mathrm{T}}\frac{\partial \hat{y}(k)}{\partial P(k)} \\ &= -\eta e(k)\left\|\frac{\partial \hat{y}(k)}{\partial P(k)}\right\|_2^2\end{aligned} \tag{18}$$

Thus,

$$\begin{aligned}\Delta L_M(k) &= -\eta e(k)\left\|\frac{\partial \hat{y}(k)}{\partial P(k)}\right\|_2^2 \cdot \left[2e(k) - \eta e(k)\left\|\frac{\partial \hat{y}(k)}{\partial P(k)}\right\|_2^2\right] \\ &= -\eta e^2(k)\left\|\frac{\partial \hat{y}(k)}{\partial P(k)}\right\|_2^2 \cdot \left[2 - \eta\left\|\frac{\partial \hat{y}(k)}{\partial P(k)}\right\|_2^2\right]\end{aligned} \tag{19}$$

Obviously, $\Delta L_M(k) < 0$ is negative-definite if and only if the sufficient condition (13) is satisfied. This completes the proof.

Moreover, the best learning rate can be found by considering at the time when $\max_k \left\|\frac{\partial \hat{y}(k)}{\partial P(k)}\right\|_2^2$ occurs. Therefore, it follows that

$$\Delta L_M(k) = -e^2(k)\max_k\left\|\frac{\partial \hat{y}(k)}{\partial P(k)}\right\|_2^2 \cdot \left[2\eta - \eta^2\max_k\left\|\frac{\partial \hat{y}(k)}{\partial P(k)}\right\|_2^2\right] \tag{20}$$

To find the best convergent rate, one finds

$$\frac{\partial \Delta L_M(k)}{\partial \eta}|_{\eta=\eta^*} = -e^2(k)\max_k\left\|\frac{\partial \hat{y}(k)}{\partial P(k)}\right\|_2^2 \cdot \left[2 - 2\eta^*\max_k\left\|\frac{\partial \hat{y}(k)}{\partial P(k)}\right\|_2^2\right] = 0 \tag{21}$$

The best convergent rate can be obtained from (21).

$$\eta^* = \frac{1}{\max_k\left\|\frac{\partial \hat{y}(k)}{\partial P(k)}\right\|_2^2}. \tag{22}$$

4 Fuzzy Distributed and Decentralized EIF Algorithm for HOMR Multi-robots

This section will develop the novel algorithm of the fuzzy distributed and decentralized extended information filtering (FDDEIF) method for HOMRs whose communication topology is not fully connected; this algorithm is different from the previous algorithm introduced in [2] for mobile multi-robot systems with a fully connected communication topology. In doing so, this section starts with the system model description of each mobile robot and graph-based model of the multi-robot system, and derive the FDDEIF algorithm.

4.1 Distributed and Decentralized Extended Information Filtering Algorithm Using a Modified Graph Theory

To cope with the cooperative localization problem of the nonlinear estimation problem from the multi-HOMR system whose communication topology is not fully connected, this subsection introduces the DDEIF algorithm with modified graph theory. Like the DEIF algorithm, the DDEIF linearizes the system state and measurement models in (4), (6) using Taylor's series expansion. In principle, the DDEIF filter takes the advantages of low computational load and ease of initialization procedure. The modified graph-based DDEIF algorithm is described as below. Suppose that interconnection topology of n HOMRs is a directed graph G, and n HOMRs can be regarded as n nodes. The relevant modified adjacency matrix is denoted as $\mathbf{A} = [a_{ij}]$, $a_{ij} \geq 0$, $\forall i, j \in \{1,2,\ldots,n\}$. Moreover we assume $a_{ii} = 1$, namely that the ith HOMR receives the localization information from its own sensors.

The modified graph-based DDEIF algorithm of the ith mobile robot is summarized as below:

(i) One-step-ahead prediction:

$$\hat{y}_i(k|k-1) = Y_i(k|k-1)f_i\big(\hat{X}_i(k-1|k-1), u_i(k-1),(k-1)\big) \tag{23}$$

$$Y_i(k|k-1) = \left[\nabla f_{X_i}(k-1)Y_i^{-1}(k-1|k-1)\nabla f_{X_i}^T(k-1) + Q_i(k-1)\right]^{-1} \tag{24}$$

where $Y_i(k|k-1)$ and $\hat{y}_i(k|k-1)$ are, respectively, the information matrix and information state vector of the ith mobile robot.

(ii) Estimation (measurement update):
At time k, the ith HOMR not only has its own measurements, but also receives the measurements of other HOMRs via the communication architecture. Hence, the measurement updates of the ith mobile robot are given by

$$\hat{y}_i(k|k) = \hat{y}_i(k|k-1) + \sum_{j=1}^{N} a_{ij}\mathbf{i}_j(k) \tag{25}$$

$$Y_i(k|k) = Y_i(k|k-1) + \sum_{j=1}^{N} a_{ij}\mathbf{I}_j(k) \tag{26}$$

where $\mathbf{I}_j(k)$ is the measurement covariance and $\mathbf{i}_j(k)$ is the measurement vector.

$$\mathbf{i}_j(k) = \nabla h_{X_j}^T(k) R_j^{-1}(k)\left[r_j(k) + \nabla h_{X_j}(k)\hat{X}(k|k-1)\right] \tag{27}$$

$$\mathbf{I}_j(k) = \nabla h_{X_j}^T(k) R_j^{-1}(k) \nabla h_{X_j}(k) \tag{28}$$

Notice that $\nabla f_{xj}(k-1)$ is the Jacobian matrix of f_j evaluated at $X_j = \hat{X}_j(k|k-1)$, $\nabla h_{xj}(k)$ is the Jacobian matrix of the output h_j evaluated at X_j, and the innovation $r_j(k)$ is given by

$$r_j(k) = Z_j(k) - h_j\left(\hat{X}_j(k|k-1)\right) \tag{29}$$

The $\nabla f_{X_j}(k-1)$ and $\nabla h_{X_j}(k)$ denote by

$$\nabla f_{X_j}(k-1) = \left.\frac{\partial f_j}{\partial X}\right|_{X=\hat{X}_j(k-1|k-1)} \tag{30}$$

$$\nabla h_{X_j}(k) = \left.\frac{\partial h_j}{\partial X}\right|_{X=\hat{X}_j(k|k-1)}. \tag{31}$$

Remark 1 If the communication topology is fully connected, then all the elements of a_{ij} are unity. For this case, modified graph-based DDEIF algorithm is reduced to the DDEIF algorithm.

4.2 Fuzzy DDEIF (FDDEIF)

The essential part of the FDDEIF is that this filter consists of N fuzzy tuners to automatically adjust its exponential weights for the measurement noise covariance matrices. Given the state Eq. (5) and measurement Eq. (6), we assume that the measurement noise covariance matrices are described by

$$R_j(k) = R_j \cdot \gamma_j^{-\kappa(k+1)}, \quad j = 1, \ldots, N \tag{32}$$

where γ_j and κ are, respectively, the weighting factor and the variation of exponential function of the ith measurement model. Note that κ is set by 2 in the paper, and γ_j is near one, and the constant matrices R_j are constant values of right dimensions. Given an initial state estimate $\hat{X}_i(0/0)$ and an initial information matrix $Y_i(0/0)$, the proposed FDDEIF whose prediction and estimation equations are modified from the exponential weighted EIF augmented with fuzzy logics in [14], which can be easily described as follows:

(i) One-step prediction:

$$\hat{y}_i(k|k-1) = Y_i(k|k-1) \times f_i\left(\hat{X}_i(k-1|k-1), U_i(k-1), (k-1)\right) \tag{33}$$

$$Y_i(k|k-1) = \left[\begin{array}{l}\gamma_i^{\kappa} \nabla f_{X_i}(k-1) Y_i^{-1}(k-1|k-1) \times \nabla f_{X_i}^T(k-1) \\ + Q_i(k-1)\end{array}\right]^{-1} \tag{34}$$

(ii) Estimation (measurement update):

$$\hat{y}_i(k|k) = \hat{y}_i(k|k-1) + \sum_{j=1}^{N} a_{ij} \nabla h_{X_j}^T(k) \left(\frac{R_j}{\gamma_j^{\kappa}}\right)^{-1} \times \left[\begin{array}{l} r_j(k) \\ + \nabla h_{X_j}(k)\hat{X}(k|k+1)\end{array}\right] \tag{35}$$

$$Y_i(k|k) = Y_i(k|k-1) + \sum_{j=1}^{N} a_{ij} \nabla h_{X_j}^T(k) \left(R_j \Big/ \gamma_j^{\kappa}\right)^{-1} \times \nabla h_{X_j}(k) \tag{36}$$

Note that if $\gamma_j = 1, j = 1, \ldots, N$, and then this FDDEIF becomes a regular DDEIF.

4.3 Fuzzy Tuner

Each fuzzy tuner for γ_j is employed to monitor the innovation to avoid divergence of the FDDEIF and to tune the value of each γ_j in (34)–(36). There are three inputs and one output for the jth fuzzy tuner. The mean value, the covariance, and covariance slew rate of the innovation of the jth fuzzy tuner are considered as the inputs to monitor the degree of filter divergence. Similar to the fuzzy tuner in [14], the three inputs of the fuzzy tuner are given as follows:

1. Statistical mean of the innovation:

$$\bar{r}_i \cong \sum_{k=1}^{l} r_i(k)/l \tag{37}$$

2. Statistical second-order moment of the innovation

$$\sigma_{r_i}^2 \cong \sum_{k=1}^{l} r_i^2(k)/l \tag{38}$$

3. The variation of the innovation second-order moment

$$\text{Slew rate} = \sigma_{r_i}^2(k) - \sigma_{r_i}^2(k-k_1). \tag{39}$$

where the parameter k_1 is positive and can be chosen by designers. Throughout the paper, we set $k_1 = 50$ and $l = 500$.

The jth fuzzy tuner uses trapezoidal membership functions for the three input variables and the output variable, and also employs five and three linguistic sets, respectively, for the statistical mean and variance of each innovation process, but adopts three linguistic sets for the output. The slew rate of the innovation variance is divided into three cases: positive, zero, and negative. Hence, 45 fuzzy rules in [14] are used for each sensor model.

5 Cooperative Pose Initialization

5.1 Landmark-Based Pose Initialization

This subsection presents a map-based initialization approach for global pose localization of one HOMR, i.e., the *i*th HOMR in the team using the measurements from the RGB-D sensor and laser scanner. For pose initialization, all the HOMRs are initially assumed to get lost in their working space, namely that all their postures of these HOMRs are unknown from the outset. To start up with the initialization procedure, all the HOMRs use their laser scanner and RGB-D sensor to accomplish collision and obstacle avoidance, and randomly navigate around the working space until any one feature or artificial landmark embedded in the environment is found by any one of the HOMRs, i.e., the *i*th HOMR. Note that the position of the feature or artificial landmark is known at a prespecified location. Once the feature or artificial landmark has been detected and then recognized by the *i*th HOMR, the position measurement, (x_{mi}, y_{mi}, z_{mi}), of the feature or landmark with respect to the RGB-D sensor mounted on the *i*th HOMR are expressed by

$$x_{mi} = x_L - x_i + v_{1i}, \quad y_{mi} = y_L - y_i + v_{2i}, \quad z_{mi} = z_L - z_i + v_{3i} \tag{40}$$

where $(x_L, y_L, z_L)^{\mathrm{T}}$ denotes the true position of the landmark; $(x_i, y_i, z_i)^{\mathrm{T}}$ represents the current position of the *i*th HOMR at the sampling instant k; v_{1i}, v_{2i}, and v_{3i} are three independent, Gaussian measurement noise processes with zero means . In order to solve the unknown position $(k-1|k-1)$ and orientation of the HOMR, it is easy to measure the relative positions of the feature or landmark using the RGB-D sensor and obtain three sets of n measured data for each feature or landmark, i.e., $x_{mi}(k)$, $y_{mi}(k)$, $z_{mi}(k)$, $k = 1, \ldots, l$. Thus, the current position of the HOMR can be estimated by the following simple averaging method.

$$x_i = x_L - \frac{1}{l}\sum_{k=1}^{n} x_{mi}(k), \quad y_i = y_L - \frac{1}{l}\sum_{k=1}^{n} y_{mi}(k), \quad z_i = z_L - \frac{1}{l}\sum_{k=1}^{n} z_{mi}(k) \tag{41}$$

5.2 Cooperative Pose Initialization

This subsection is aimed at finding the initial poses of other $n-1$ HOMRs if the *i*th HOMR is self-localized by recognizing and measuring a RGB-D-based feature, landmark, and its surrounding environment model. In the cooperative localization scenario, if the *j*th HOMR is detected by the laser scanner in the *i*th HOMR, then it is easy to find that the distance between both HOMRs is d_{ij}, and the angle between the line-of-sight and the heading of the *i*th HOMR is ϕ_{ij} (positive in the counterclockwise (CCW) direction and negative in the clockwise (CW) direction. Therefore, then the position of the *j*th HOMR is calculated by the following equations:

$$x_j = x_i + d_{ij}\cos(\phi_{ij} + \theta_i), y_j = y_i + d_{ij}\sin(\phi_{ij} + \theta_i) \tag{42}$$

Once the position of the *j*th HOMR has been determined, then the heading of the *j*th HOMR can be found by using the following cases:

Case 1 If the *j*th HOMR can observe and identify the L neighboring walls using its own laser scanner and map, then orientation of the *j*th HOMR is averagely computed by

$$\theta_j = \left(\sum_{k=1}^{L} \beta_k^m - \beta_k/L\right) \tag{43}$$

Case 2 If a RGB-D-based landmark can be found by the *j*th HOMR, then its orientation is easily calculated by

$$\theta_j = \tan 2^{-1}\frac{y_L - y_j}{x_L - x_j} - \alpha_j \tag{44}$$

where $\alpha_j = \tan 2^{-1}(y_j/x_j)$ is the azimuth angle between the detected landmark and RGB-D sensor.

Remark 2 Assume that the communication network is connected. The proposed cooperative initialization method based on the two cases is shown effective in finding all the initial pose estimations of all the robots.

6 BLS-FDDEIF for Dynamic Localization

This section is devoted to describing the main ideas of the proposed cooperative BLS-FDDEIF localization method for the moving multi-HOMR system. By considering the directed communication network among these multi-robots, this section will apply the BLS-FDDEIF algorithm to the multi-HOMR system including three kinds of omnidirectional wheeled mobile robots. By including the previous cooperative pose initialization algorithm, this section will develop a discrete-time BLS-FDDEIF dynamic pose estimation method to obtain the best pose estimate of each HOMR when the multiple HOMRs navigate around their indoor working environments and some of embedded landmarks can be observed by HOMRs. Figure 3 depicts the block diagram of the BLS-FDDEIF algorithm for each HOMR. The discrete-time BLS-FDDEIF dynamic pose estimation is described in the following six steps.

Step 1: Measure the relative position of one landmark using the RGB-D sensor and obtain one set of n measured data for each landmark, i.e., $x_{mi}(l), y_{mi}(l), z_{mi}(l)$, $l = 1, \ldots, n$.

Step 2: Use (41) and cooperative pose initialization method to solve for the start-up position $(x_i(k), y_i(k), z_i(k))^{\mathrm{T}}$ and initial orientation $\theta_i(k)$ of the ith HOMR.
Step 3: Select the initial values of each information state $\hat{y}_i(0|0)$ and information matrix $Y_i(0|0)$ at time k $k = 0$ for each HOMR.
Step 4: Do the one-step prediction by setting each optimal information state estimate and the information matrix at time $k-1$ to be $\hat{y}_i(k-1|k-1)$ and $Y_i(k-1|k-1)$ using (32, 33) and use each BLS to learn each $\mathbf{g}_i$ in real time.
Step 5: Obtain the updating estimate $\hat{y}_i(k|k)$ and the information matrix $Y_i(k|k)$ at time k using (35, 36) where the fuzzy tuner is used and each HOMR reads the N-pairs measurement data $Z_j(k)$, $j = 1, \ldots, N$.
Step 6: Repeat Steps 4 and 5.

7 Simulations and Discussion

In this section, three simulations are performed to examine the performance and merits of the proposed cooperative pose initialization and BLS-FDDEIF dynamic pose tracking method for the multi-HOMR system in [13]. Each HOMR is equipped with encoders amounted on the driving wheels, one laser scanner and one RGB-D sensor. The first simulation verifies the proposed cooperative pose initialization algorithm, and the second simulation aims to accomplish the BLS-FDDEIF algorithm for dynamic pose tracking. The third simulation is employed to compare the superiority of the BLS-FDDEIF by comparing to BLS-DDEIF. Three simulations are done by using MATLAB/Simulink under the case in which the three HOMRs navigate in a flat terrain in structured environments where all the landmarks are well recognized. In three simulations, both two landmarks in the surrounding space are, respectively, installed at (x_{L1}, y_{L1}, z_{L1}) = (5 m, 2 m, 2 m) and (x_{L2}, y_{L2}, z_{L2}) = (5 m, 3 m, 2 m); the parameters of the walls are given by (ρ_1^m = 0, β_1^m = 90°), (ρ_2^m = 5, β_2^m = 0°), (ρ_3^m = 5, β_3^m = 90°).

In the first simulation, the true poses of the three HOMRs are, respectively, set (2 m, 1.5 m, 1 m, 0°), (3 m, 2.5 m, 1 m, 0°), (3.5 m, 3.5 m, 1 m, 0°). Figure 4 depicts the simulation results where the black circles are the true positions and the green circles denote the estimated position. The results in Fig. 4a reveal that the initial posture estimates are very close to their true values. In the first simulations, we assume that the first HOMR can recognize two landmarks, the three walls, and use FDDEIF to fuse these data to obtain the estimated pose. The second HOMR cannot detect one of the landmarks, so the first HOMR can transmit that information for the second HOMRs. The third HOMR is localized by the second HOMR using the laser scanner to measure the distance and angle between the two HOMRs. Figure 4b shows that when high noise occurs during the measurements of each HOMR, BLS-FDDEIF can avoid the divergence of pose estimation of each HOMRs. Table 1 displays the root mean-square errors (RMSEs) of the initial posture estimates of the three HOMRs for the high noise case, where the performance index, RMSE, is defined by RMSE = $\sqrt{\sum_i^n (x_{ei}^2 + y_{ei}^2 + \theta_{ei}^2)} \Big/ n$.

The second simulation aims to investigate the effectiveness of the proposed BLS-FDDEIF method for dynamic pose tracking of the three HOMRs where they are moving 1 m along the x-axis and the simulation environment is identical to Simulation 1, as shown in Fig. 4a. The red HOMR uses the car-like omnidirectional dynamic

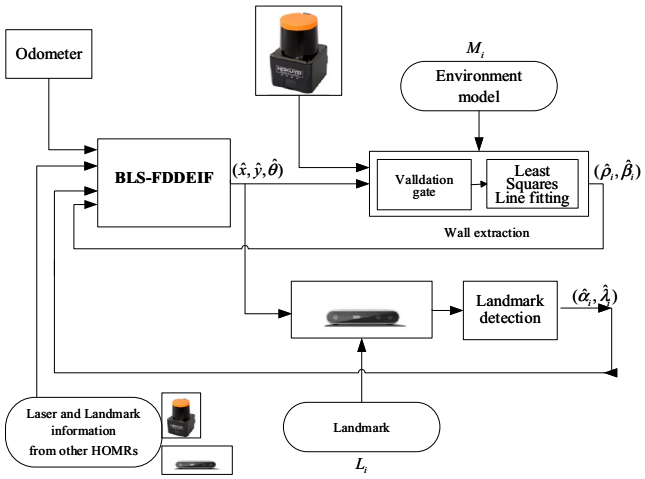

Fig. 3 Block diagram of the BLS-FDDEIF algorithm for each HOMR

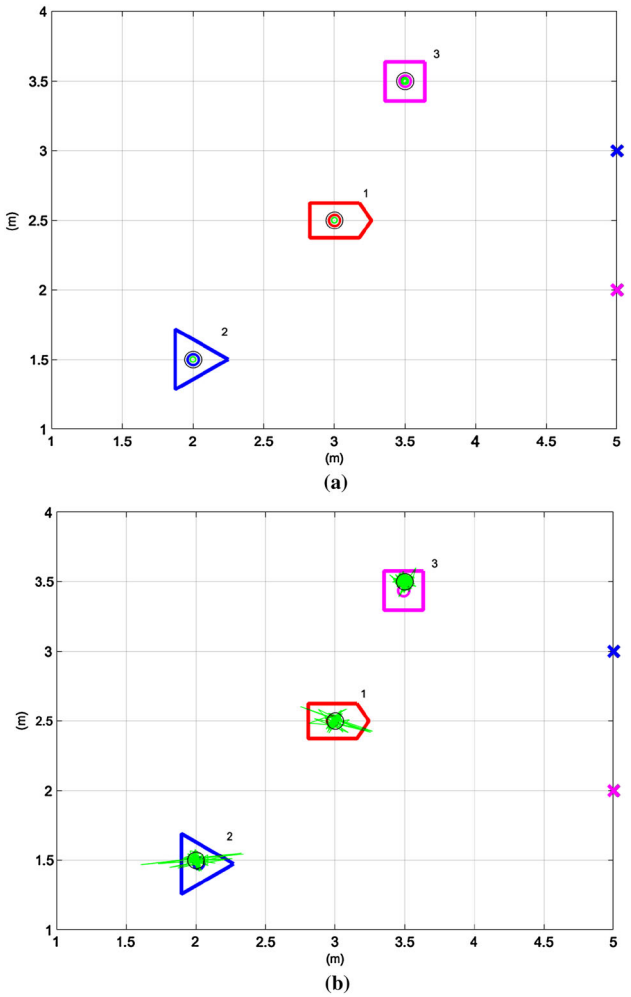

Fig. 4 Environment settings and results of the first simulation for high noise case: **a** little measurement noise; **b** big measurement noise

model, the blue HOMR adopts the three-wheeled omnidirectional dynamic model, and the pink HOMR exploits the four-wheeled omnidirectional dynamic model. All the three HOMRs are moving 1 m along the x-axis. Figure 5 depicts the simulation results of the three HOMRS when the measurement data are corrupted with little noise, thereby showing the effectiveness of the proposed BLS-FDDEIF localization method. Table 2 compares the RMSEs of estimated poses of the two algorithms, BLS-FDDEIF and FDDEIF, for dynamic pose tracking in the second simulation.

Table 1 List of the root mean-square errors (RMSEs) of the initial posture estimates of the three HOMRs for high noise case

HOMR	Index RMSE
COMR	0.0534
TOMR	0.0649
FOMR	0.0712

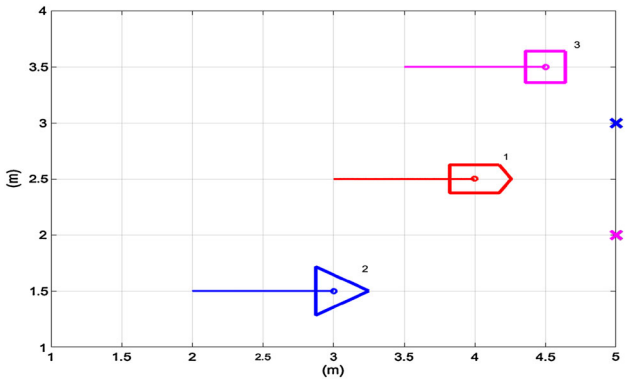

Fig. 5 Dynamic pose tracking simulation of the cooperative BLS-FDDEIF localization algorithm

Table 2 List of the RMSEs of pose tracking in second simulation

HOMR	Controller		
	BLS-FDDEIF	FDDEIF	Improvement (%)
COMR	0.0725	0.1122	54.76
TOMR	0.0303	0.0441	46.51
FOMR	0.0549	0.0592	7.83

The results in Table 2 indicate that the BLS-FDDEIF is superior to the FDDEIF in terms of RMSEs. Table 3 compares the RMSEs of the estimated velocities from the two algorithms, BLS-FDDEIF and FDDEIF, in the second simulation, Table 3 reveals that the BLS-FDDEIF is still superior to FDDEIF in terms of RMSEs of estimated velocities of the three HOMRs.

The third simulation is used to compare the BLS-DDEIF and BLS-FDDEIF methods in estimated position accuracy of the three HOMRs where they are moving 0.5 m along the x-axis and the big measurement noise as shown in Fig. 6. The same color lines display the estimated positions using the BLS-DDEIF algorithm, while the green lines illustrate the estimated positions using BLS-FDDEIF. Tables 4 and 5 present the comparative RMSEs of the pose tracking and velocity tracking errors using the two algorithms in the third simulation for the high noise case.

Table 3 List of the RMSEs of the estimated velocities of the three HOMRS in the second simulation

HOMR	Controller		
	BLS-FDDEIF	FDDEIF	Improvement (%)
COMR	0.0118	0.0126	6.78
TOMR	0.0122	0.0129	5.74
FOMR	0.0125	0.0132	5.6

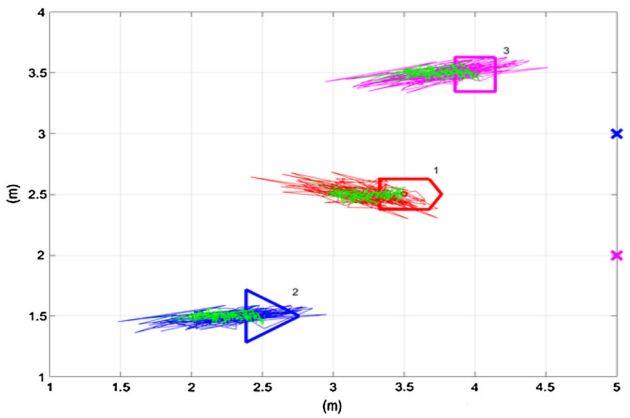

Fig. 6 Comparative time evolutions of the true poses and BLS-DDEIF and BLS-FDDEIF estimated positions of the three HOMRs for high noise case

Table 4 List the RMSEs of the pose tracking errors of the three HOMRs in the third simulation for high noise case

HOMR	Controller		
	BLS-FDDEIF	BLS-DDEIF	Improvement (%)
COMR	0.0546	0.1957	258.42
TOMR	0.0633	0.2211	249.29
FOMR	0.0707	0.2161	205.66

Table 5 Comparison of the RMSEs of estimating velocities the three HOMRs using the two algorithms, BLS-FDDEIF and BLS-DDEIF in the third simulation

HOMR	Controller		
	BLS-FDDEIF	BLS-DDEIF	Improvement (%)
COMR	0.017	0.0176	3.53
TOMR	0.0208	0.022	5.77
FOMR	0.0213	0.022	3.28

Obviously, the results reveal that BLS-FDDEIF significantly outperforms BLS-DDEIF in terms of improvement percentages.

8 Experimental Results and Discussion

This section conducts two experiments to verify the real performance and applicability of the proposed cooperative BLS-FDDEIF localization algorithm. Figure 7 illustrates the three experimental HOMRs and the experimental environment with one landmark was installed at (x_{L1}, y_{L1}, z_{L1}) = (2 m, 1.17 m, 0.25 m), and three walls were given by $(\rho_1^m = 0, \beta_1^m = 90°)$, $(\rho_2^m = 5, \beta_2^m = 0°)$, $(\rho_3^m = 5, \beta_3^m = 90°)$, respectively. In the beginning, the first robot was stopped at (1 m, 1.17 m), the second robot was initialized at (0.5 m, 1.67 m), and the third robot got started at (0.5 m, 0.67 m). Note that all the three robots did not have their initial true poses with respect to their surroundings. Therefore, the Realsense RGB-D sensor was used to detect the surrounding landmark, and the laser scanner was exploited to measure the perpendicular distances and orientations of the walls.

Fig. 7 Three experimental HOMRs and experimental environment

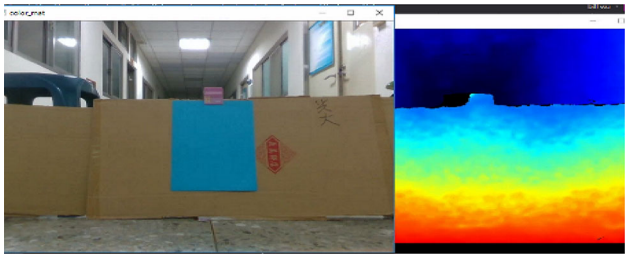

Fig. 8 The color and depth image from Realsense RGB-D sensor

For landmark detection, one used color feature extractions to locate its center point. Figure 8 illustrates the color and depth image from the RealSense RGB-D sensor, and Fig. 9 displays the extracted blue blocks by removing other colors by using the HSV color space. Moreover, Fig. 10 indicates the contour of the chosen biggest blue block.

In the first experiment when all the HOMRS were stopped at their initial points, each HOMR used its onboard RGB-D camera to detect the relative position between the landmark and itself, and, meanwhile, utilized its onboard laser scanner to measure the perpendicular distance ρ_j and orientation β_j of each wall in the robot frame. By taking the BLS-FDDEIF algorithm to fuse the readings from these RGB-D sensors and laser scanners, the estimated positions of the three HOMRS were, respectively, found by (1.005 m, 1.1734 m), (0.4964 m, 1.6663 m), and (0.4978 m, 0.6787 m). Moreover, the statistically estimated errors of the three corresponding HOMRs were given by (0.0005 m, 0.0034 m), (0.0036 m, 0.0037 m), and (0.0022 m, 0.0087 m), respectively. These results indicate that the proposed BLS-FDDEIF algorithm worked well for this scenario.

Fig. 9 Extracted blue blocks from the Realsense RGB-D sensor

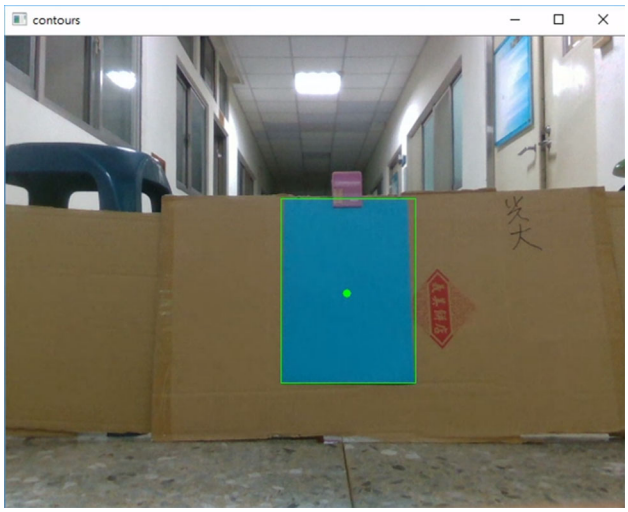

Fig. 10 Illustration of the largest selected blue block from the Realsense

The second experiment is carried out to explore the real performance of the proposed cooperative BLS-FDDEIF dynamic localization method for the three HOMRs. The experimental set-up was identical to the first experiment but all the three HOMRs moved along a slant line. The BLS-FDDEIF algorithm was coded by standard C programming language. Figure 11 shows the experimental pictures during the second experimental process in which all the three HOMRs moved 0.4 m along the x-axis defined in the world frame. Figure 12 demonstrates the experimental estimates of dynamic poses of the three moving HOMRs. Moreover, Table 6 displays their RMSEs, respectively. Through the experiment results in Table 6, the proposed BLS-FDDEIF algorithm has been shown applicable and practicable in achieving cooperative localization of the multi-HOMR system.

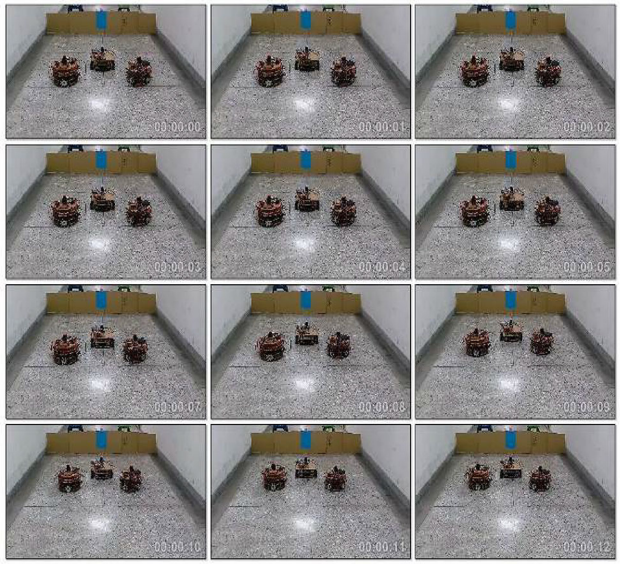

Fig. 11 Experimental pictures of the cooperative dynamic localization of the three moving HOMRs

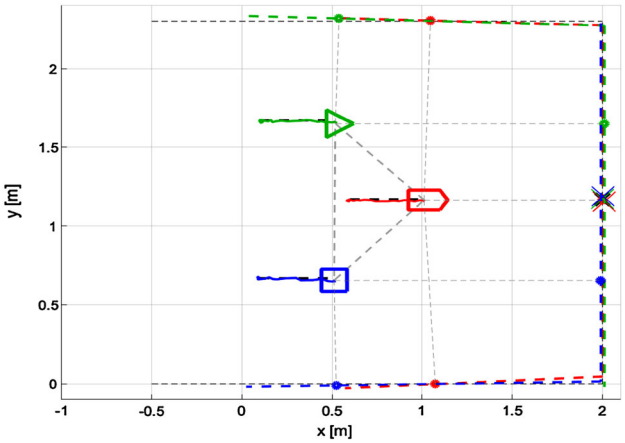

Fig. 12 Experimental results of the cooperative dynamic pose estimates of the three moving HOMRs

Table 6 List of the RMSEs of the dynamic pose estimates of the three moving HOMRs

HOMR	Index RMSE
COMR	0.0271
TOMR	0.0395
FOMR	0.0361

9 Conclusions and Future work

This paper has presented a novel FDDEIF method augmented by broad learning system (BLS), called BLS-FDDEIF, for cooperative pose initialization and dynamic pose tracking of a team of heterogeneous omnidirectional mobile robots (HOMRs). Each BLS with its iterative

gradient decent algorithm has been proposed to approximate the dynamic effects and uncertainty vectors in the dynamic model of each HOMR in real time. By fusing measurement information taken from the encssoders, RGB-D sensor, and laser scanner, the proposed static global pose initialization and BLS-FDDEIF dynamic pose estimation methods have been shown capable of obtaining accurate pose and pose rate estimates of the HOMRs. Comparative simulation results have demonstrated the effectiveness and superiority of the proposed BLS-FDDEIF method for a group of HOMRs. The practicability of the proposed BLS-FDDEIF method has been well demonstrated by conducting static and dynamic experiments using the three cooperating HOMRs. An interesting topic for future research would be to develop a fuzzy distributed decentralized extended Kalman filtering (FDDEKF) localization using BLS, abbreviated as BLS-FDDEKF, for cooperative pose initialization and dynamic pose tracking of the multi-HOMR system owing to direct estimation of the physical state variables instead of information state variables.

Acknowledgements The authors deeply acknowledge financial support from Ministry of Science and Technology (MOST), Taiwan, ROC, under contract MOST 107-2221-E-005-073-MY2.

References

1. Parker, L.E.: Distributed intelligence: overview of the field and its application in multi-robot systems. J. Phys. Agents **2**(1), 1–14 (2008)
2. Tsai, C.C., Chan, C.C., Tai, F.C.: Cooperative localization using fuzzy decentralized extended information filtering for homogenous omnidirectional mobile multi-robot system. In: Proc. of 2015 Intern. Conf. on Syst. Science and Eng., Morioka, Japan, 6–8 July, 2015
3. Tan, Y.M.: Fuzzy decentralized cooperative global localization for a multi-ballbot system. MS Thesis, Department of Electrical Engineering, National Chung Hsing University (2016)
4. Yang, G.H.: Cooperative global pose estimation and localization for a heterogeneous omnidirectional multirobot system using fuzzy distributed and decentralized filtering. MS Thesis, Department of Electrical Engineering, National Chung Hsing University (2018)
5. Wang, Y., de Silva, C.W.: Sequential Q-Learning with Kalman filtering for multirobot cooperative transportation. IEEE/ASME Trans. Mechatron. **15**(2), 261–268 (2010)
6. Kuo, C.W., Tsai, C.C.: Quaternion-based adaptive backstepping RFWNN control of quadrotors subject to model uncertainties and disturbances. Int. J. Fuzzy Syst. **20**(6), 1745–1755 (2018)
7. Chen, C.L.P., Liu, Z.L., Feng, S.: An effective and efficient incremental learning system without the need for deep architecture. IEEE Trans. Neural Netw. Learn. Syst. **29**(1), 10–24 (2018)
8. Chen, C.L.P., Liu, Z.L., Feng, S.: A new paradigmatic broad learning system: structural variations and universal approximation capability. IEEE Trans. Neural Netw. Learn. Syst. **30**(4), 1191–1204 (2019)
9. Feng, S., Chen, C.L.P.: Broad learning system for control of nonlinear dynamic systems. In: 2018 IEEE Intern. Conf. on Systems, Man, and Cybernetics, Miyazaki, Japan, 7–10 October 2018
10. Tsai, C.C., Yu, C.C., Wu, C.W.: Adaptive distributed BLS-FONTSM formation control for uncertain networking heterogeneous omnidirectional mobile multirobots. J. Chin. Inst. Eng. (2019)
11. Indiveri, G.: Swedish wheeled omnidirectional mobile robots: kinematics analysis and control. IEEE Trans. Robot. **25**(1), 164–171 (2009)
12. Tsai, C.C., Wu, H.L., Tai, F.C., Chen, Y.S.: Distributed consensus formation control with collision and obstacle avoidance for uncertain networked omnidirectional multi-robot systems using fuzzy wavelet neural networks. Int. J. Fuzzy Syst. **19**(5), 1375–1391 (2017)
13. Tsai, C.C., Tai, F.C., Feng, K.H.: Fuzzy sliding-mode consensus formation control of networked heterogeneous Mecanum-wheeled multirobots with dynamic effects. In: Proc. of 2018 IEEE Intern. Conf. on Fuzzy Systems (FUZZ-IEEE 2018), Rio de Janeiro, Brazil, 8–13 July 2018
14. Lin, H.H., Tsai, C.C.: Ultrasonic localization and pose tracking of an autonomous mobile robot via fuzzy adaptive extended information filtering. IEEE Trans. Instrum. Meas. **57**(9), 2024–2034 (2008)

Ching-Chih Tsai has done his Diploma in Electrical Engineering from National Taipei Institute of Technology, Taipei, Taiwan, ROC; M.S. in Control Engineering from National Chiao Tung University, Hsinchu, Taiwan, ROC; and Ph.D. in Electrical Engineering from Northwestern University, Evanston, IL, USA, in 1981, 1986, and 1991, respectively. He has published and coauthored over 500 technical papers, and is currently a life distinguished professor in the Department of Electrical Engineering, National Chung Hsing University, Taichung, Taiwan, ROC. From 2003 to 2005, he served as the Director at Center for Research Development and Engineering Technology, College of Engineering, National Chung Hsing University. In 2006, he served as the Chair, Taipei chapter, IEEE Robotics and Automation Society, and the Director at Center for Advanced Industry Technology and Precision, National Chung Hsing University. Since 2009, he has been the Chair, Taichung Chapter, IEEE Systems, Man and Cybernetics Society (SMCS). From 2012 to 2016, he served two terms of the President, the Chinese Automatic Control Society, Taiwan. Since 2016, he has served as the President of Robotics Society of Taiwan, and the Vice President of International Fuzzy Systems Association. He is a Fellow of IEEE, IET, Chinese Automatic Control Society and Robotics Society of Taiwan. His current research interests include advanced control methods, intelligent control, embedded control systems, and their applications to industrial processes and intelligent mobile robots.

Ching-Fu Hsu has received his B.S. degree in the Department of Electronic Engineering from Chienkuo Technology University in 2001 and M.S. degree in the Department of Computer Science and Information Engineering from Chaoyang University of Technology in 2003, respectively. From 2003 to 2015, he served as a project leader in Taiwan Wintek Corp. Since 2015, he has been with Taiwan ASUS Computer Corp. Currently, he is working towards his Ph.D. degree in the Department of Electrical Engineering, National Chung Hsing University, Taichung, Taiwan. His current interests include image processing, display driving technology, robotic vision, and their applications to touch/display modules and service robots.

Chung-Wei Wu has received his M.S. degree in the Department of Electrical Engineering from National Chung Hsing University, Taichung, Taiwan, ROC, in 2019. His current research interests include mobile robots and intelligent control.

Feng-Chun Tai has received his B.S., M.S., and Ph.D. degrees in the Department of Electrical Engineering from National Chung Hsing University, Taichung, Taiwan, ROC. in 2007, 2010, and 2018, respectively. His current research interests include mobile robots, intelligent control, navigation system, and their applications to industrial processes and machines.